UCSF

UC San Francisco Previously Published Works

Title

Contractility of single cardiomyocytes differentiated from pluripotent stem cells depends on physiological shape and substrate stiffness.

Permalink

https://escholarship.org/uc/item/7cp9q4h5

Journal

Proceedings of the National Academy of Sciences of USA, 112(41)

Authors

Ribeiro, Alexandre

Ang, Yen-Sin

Fu, Ji-Dong

et al.

Publication Date

2015-10-13

DOI

10.1073/pnas.1508073112

Peer reviewed

eScholarship.org Powered by the California Digital Library
University of California

Contractility of single cardiomyocytes differentiated from pluripotent stem cells depends on physiological shape and substrate stiffness

Alexandre J. S. Ribeiro[a,b], Yen-Sin Ang[c,d], Ji-Dong Fu[c,d,1], Renee N. Rivas[c,d], Tamer M. A. Mohamed[c,d,e], Gadryn C. Higgs[a,b], Deepak Srivastava[c,d,f,g], and Beth L. Pruitt[a,b,h,2]

[a]Department of Mechanical Engineering, Stanford University, Stanford, CA 94305; [b]Stanford Cardiovascular Institute, Stanford University, Stanford, CA 94305; [c]Gladstone Institute of Cardiovascular Disease, San Francisco, CA 94158; [d]Roddenberry Center for Stem Cell Biology and Medicine at Gladstone Institutes, San Francisco, CA 94158; [e]Institute of Cardiovascular Sciences, University of Manchester, Manchester M13 9PT, United Kingdom; [f]Department of Pediatrics, University of California, San Francisco, CA 94143; [g]Department of Biochemistry & Biophysics, University of California, San Francisco, CA 94143; and [h]Department of Molecular and Cellular Physiology, Stanford University, Stanford, CA 94305

Edited by James A. Spudich, Stanford University School of Medicine, Stanford, CA, and approved August 26, 2015 (received for review May 1, 2015)

Single cardiomyocytes contain myofibrils that harbor the sarcomere-based contractile machinery of the myocardium. Cardiomyocytes differentiated from human pluripotent stem cells (hPSC-CMs) have potential as an in vitro model of heart activity. However, their fetal-like misalignment of myofibrils limits their usefulness for modeling contractile activity. We analyzed the effects of cell shape and substrate stiffness on the shortening and movement of labeled sarcomeres and the translation of sarcomere activity to mechanical output (contractility) in live engineered hPSC-CMs. Single hPSC-CMs were cultured on polyacrylamide substrates of physiological stiffness (10 kPa), and Matrigel micropatterns were used to generate physiological shapes (2,000-μm^2 rectangles with length:width aspect ratios of 5:1–7:1) and a mature alignment of myofibrils. Translation of sarcomere shortening to mechanical output was highest in 7:1 hPSC-CMs. Increased substrate stiffness and applied overstretch induced myofibril defects in 7:1 hPSC-CMs and decreased mechanical output. Inhibitors of nonmuscle myosin activity repressed the assembly of myofibrils, showing that subcellular tension drives the improved contractile activity in these engineered hPSC-CMs. Other factors associated with improved contractility were axially directed calcium flow, systematic mitochondrial distribution, more mature electrophysiology, and evidence of transverse-tubule formation. These findings support the potential of these engineered hPSC-CMs as powerful models for studying myocardial contractility at the cellular level.

contractility | sarcomeres | cardiomyocyte | stem cell | single cell

Myocardial contractility is essential for heart function. Disruption of the contractile activity of heart muscle cells, cardiomyocytes (CMs), can lead to heart disease, and altering CM contractility is a common approach to treating a failing heart (1). Single CMs contain all of the machinery involved in myocardial contractility (2), which consists of sarcomeres in series that shorten along myofibrils as a result of myosin activity (3). Sarcomeric myosins convert the chemical energy of ATP into mechanical energy (4) upon binding to actin thin filaments and promote sarcomere shortening. Each sarcomere occupies the space between Z lines (5), and collective shortening of sarcomeres translates to mechanical output in the CM contractile cycle.

CMs differentiated from human pluripotent stem cells (hPSC-CMs) have potential for studying heart disease (6). Specifically, hPSC-CMs can model myocardial physiology in vitro (7). hPSC-CMs may be better in vitro models of contractility than neonatal or mature murine primary CMs, because they can be maintained in culture longer (2) and because the sarcomeric contractile machinery differs between human and murine CMs (8, 9). However, hPSC-CMs derived from current differentiation protocols present myofibril alignment resembling that of fetal CMs, limiting their ability to replicate the contractility of primary adult CMs (6).

Microfabrication techniques can engineer hPSC-CMs to develop systems in which cell properties and function match physiological properties (10, 11). Engineered multicellular cultures of hPSC-CMs can model cardiac contractility (10, 11) but are limited by cell-to-cell variations in myocyte type (atrial, ventricular, and nodal), cell size, shape, and myofibril alignment, which can lead to inaccurate measurements of contractile output (12).

To create a mature alignment of myofibrils, we cultured single hPSC-CMs on polyacrylamide substrates of physiological stiffness (10 kPa) (13) with rectangular 2,000-μm^2 Matrigel micropatterns and aspect ratios (length to width) of 3:1–7:1. Matrigel is an extracellular matrix mixture (14), and CMs assume the shape of micropatterns of extracellular proteins printed on surfaces (11, 15, 16). A rectangular shape of hPSC-CMs with a physiological aspect ratio of 7:1 and area of 2,000 μm^2 engineers a physiological organization of sarcomeres (11), with myofibrils aligned along the main cell axis, as in primary adult murine CMs (17). Culturing primary neonatal murine CMs on substrates with a physiological stiffness (~10 kPa) leads to mature myofibril organization and cell function (13, 18).

Significance

Human cardiomyocytes differentiated from pluripotent stem cells (hPSC-CMs) have potential as in vitro models of cardiac health and disease but differ from mature cardiomyocytes. In single live engineered hPSC-CMs with physiological shapes, we assayed the mechanical output and activity of sarcomeres and myofibrils in a nondestructive, noninvasive manner. Substrates with physiological stiffness improved contractile activity of patterned hPSC-CMs, as well as calcium flow, mitochondrial organization, electrophysiology, and transverse-tubule formation. The mechanical output and activity of sarcomeres and myofibrils varied as a function of mechanical cues and disrupted cell tension. This study establishes a high-throughput platform for modeling single-cell cardiac contractile activity and yields insight into environmental factors that drive maturation and sarcomere function in hPSC-CMs.

Author contributions: A.J.S.R., Y.-S.A., G.C.H., D.S., and B.L.P. designed research; A.J.S.R., Y.-S.A., J.-D.F., and R.N.R. performed research; A.J.S.R., Y.-S.A., R.N.R., and T.M.A.M. contributed new reagents/analytic tools; A.J.S.R., Y.-S.A., J.-D.F., D.S., and B.L.P. analyzed data; and A.J.S.R., D.S., and B.L.P. wrote the paper.

The authors declare no conflict of interest.

This article is a PNAS Direct Submission.

[1]Present address: Heart and Vascular Research Center, Department of Medicine, MetroHealth Campus, Case Western Reserve University, Cleveland, OH 44120.

[2]To whom correspondence should be addressed. Email: pruitt@stanford.edu.

This article contains supporting information online at www.pnas.org/lookup/suppl/doi:10.1073/pnas.1508073112/-/DCSupplemental.

CELL BIOLOGY

In this study, we analyzed the contractile mechanical output of single engineered rectangular hPSC-CMs (11) on 10-kPa hydrogels as a function of sarcomere shortening and myofibril organization. Our goals were (*i*) to determine whether sarcomere activity affects contractility as a function of cell shape and substrate stiffness, and (*ii*) to understand how these cues regulate contractility. We calculated the mechanical output of beating hPSC-CMs and simultaneously imaged fluorescently labeled actin to quantify myofibril organization and sarcomere dynamics. We then tested the effects of substrate stiffness and subcellular tension on the mechanical output and myofibril organization of engineered hPSC-CMs. We also assayed calcium flow, mitochondrial organization, electrophysiology, and the presence of transverse-tubule (t-tubule) structures.

Results

Increased Myofibril Alignment Improves Sarcomere Activity and Mechanical Output. To induce a mature alignment of myofibrils in single hPSC-CMs on 10-kPa polyacrylamide substrates (*SI Appendix*, Fig. S1 and *SI Materials and Methods*), we cultured hPSC-CMs on rectangular 2,000-μm^2 Matrigel micropatterns with aspect ratios of 3:1–7:1. Single hPSC-CMs attached to the micropatterns and assumed their shapes (Fig. 1*A*, *SI Appendix*, Fig. S2, and Movies S1 and S2). Unpatterned hPSC-CMs and hPSC-CMs on square patterns (1:1) with a constant area of 2,000 μm^2 were also cultured (Fig. 1). To reveal sarcomeres along myofibrils (Fig. 1*B* and *SI Appendix*, Fig. S3), we labeled F-actin with Lifeact (19). Increasing the aspect ratio of patterns progressively increased myofibril alignment (Fig. 1*B*). In these engineered hPSC-CMs, sarcomeres laterally registered with sarcomeres in neighboring myofibrils, inducing intersarcomeric alignment of Z lines perpendicular to the direction of myofibril alignment (*SI Appendix*, Fig. S2), as in patterned neonatal murine CMs (20, 21) and hPSC-CMs patterned on glass (11). However, in unpatterned and square hPSC-CMs, myofibrils had random directionality.

The sum of hPSC-CM contractile force magnitudes ($\Sigma|F_c|$) (Figs. 1*C* and 2*A*), work, and power (*SI Appendix*, Fig. S4) increased with cell aspect ratio. Unpatterned contractile cells had random shapes, and their $\Sigma|F_c|$ increased with adhesion area (*SI Appendix*, Fig. S5*A*). Unpatterned ~2,000-μm^2 hPSC-CMs had the same $\Sigma|F_c|$ as 1:1 hPSC-CMs. Unpatterned >2,000-μm^2 hPSC-CMs generated $\Sigma|F_c|$ similar to 3:1 engineered hPSC-CMs. Aspect ratio did not affect the mean cell-shortening velocity (*SI Appendix*, Fig. S5*B*). Because power scales with velocity, differences in the power output of these cells mainly reflected differences in $\Sigma|F_c|$. In engineered hPSC-CMs, power varied exponentially with $\Sigma|F_c|$, independent of aspect ratio (*SI Appendix*, Fig. S5*C*). Calculation of the maximal velocity of microbead displacement during cell contraction (V_C) and cell relaxation (V_R) showed that V_C and V_R increased with the cell aspect ratio (*SI Appendix*, Fig. S5*D*), possibly due to differences in cell contractility. Evidently, improved sarcomere activity drives the greater mechanical output of engineered hPSC-CMs.

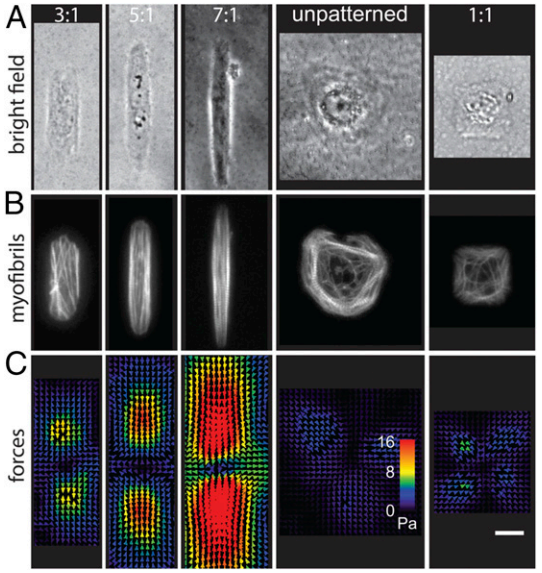

Fig. 1. Matrigel micropatterns on traction-sensitive polyacrylamide hydrogel devices constrain hPSC-CMs to controllable shapes and engineer their mechanical output. Each row of images shows the same cell. Dimensions are similar for all images. Cells were cultured on micropatterns to induce aspect ratios of 1:1–7:1 and areas of 2,000 μm^2. (*A*) Cells imaged with bright-field microscopy. (*B*) Lifeact-labeled actin in myofibrils in live hPSC-CMs. (*C*) Heat maps of maximal substrate traction during cell contraction are estimated with traction force microscopy. (Scale bar, 20 μm.)

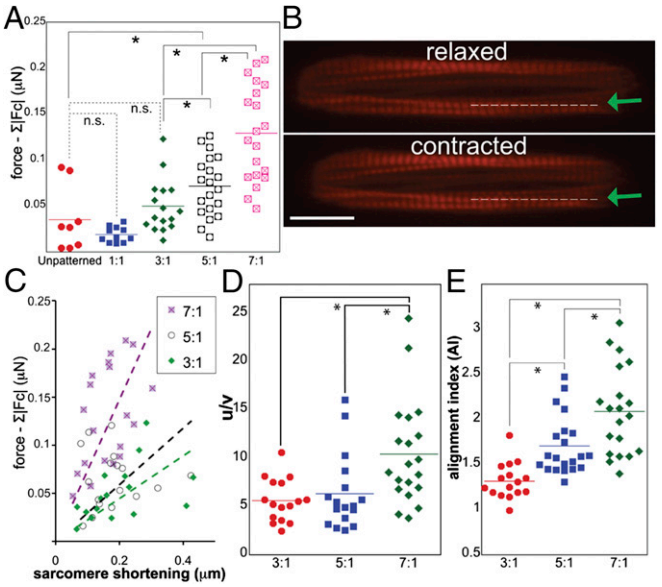

Fig. 2. Myofibril alignment leads to higher contractile forces in single hPSC-CMs. (*A*) $\Sigma|F_c|$ of engineered hPSC-CMs increases with cell aspect ratio. (*B*) Sarcomere length during contraction and relaxation calculated in Lifeact-labeled cells from intensity profile of line scans (dotted line with green arrow) along myofibrils. (Scale bar, 20 μm.) (*C*) Sarcomere shortening leads to higher $\Sigma|F_c|$ in 7:1 cells than in cells with other aspect ratios. (*D*) The ratio of myofibril movement along the major axis of the cell (u) to myofibril movement along the minor axis of the cell (v) increases as aspect ratio increases. (*E*) Alignment index of hPSC-CMs with different aspect ratios. Alignment of myofibrils increases with the aspect ratio of hPSC-CMs. ANOVA P value < 0.001 (*A*, *D*, and *E*). *P < 0.01 by unpaired Wilcoxon–Mann–Whitney rank-sum test and by Bonferroni's all pairs comparison test; n.s., not significant. Each point indicates one cell. In *A*, *D*, and *E*, lines denote the mean.

To simultaneously measure the mechanical output and dynamics of sarcomeres, we acquired videos of engineered hPSC-CMs with Lifeact-labeled (19) myofibrils contracting under electrical field stimulation at 1 Hz (Fig. 2*B* and Movies S3 and S4). Labeling did not alter $\Sigma|F_c|$ (*SI Appendix*, Fig. S6*A*). Sarcomere shortening was calculated as the difference between sarcomere length when hPSC-CMs were contracted and relaxed (Fig. 2*B* and *SI Appendix*, Fig. S7). Interestingly, $\Sigma|F_c|$ per μm of shortening increased with cell

aspect ratio (Fig. 2*C*), whereas sarcomere shortening remained constant with aspect ratio (*SI Appendix*, Fig. S6*B*). Thus, we asked whether myofibril and sarcomere alignment increased with aspect ratio to more efficiently translate sarcomere shortening to mechanical output.

Using particle-tracking velocimetry, we quantified myofibril movement in 7:1 engineered hPSC-CMs along the cell major (x) and minor axes (y) (*SI Appendix*, Fig. S8) by tracking actin movement between the relaxed and contracted states. We then calculated the displacement ratio $[u(x)/v(y)]$ of myofibrils for single hPSC-CMs with different aspect ratios (Fig. 2*D*). Overall movement of myofibrils along the major axis was greatest in 7:1 hPSC-CMs. Increased myofibril motion $[u(x)]$ and increased myofibril alignment induced sarcomere shortening to maximize the axial contractile output of engineered hPSC-CMs. High myofibril alignment along the major axis is a hallmark of CM maturity (6), and the myofibril alignment index (AI) also increased with the aspect ratio (Fig. 2*E*).

Cell Shape and Substrate Stiffness Coordinate the Contractile Machinery by a Tuned Tension Mechanism. Along with cell shape, substrate stiffness affects the cytoskeleton (23) and mechanical phenotypes of cells (24, 25) and may regulate the mechanical output of engineered hPSC-CMs. Generally, tension along the cell membrane increases with the aspect ratio of adherent cells (26). Intracellular tension also increases with substrate stiffness (27, 28), and the contractility of primary neonatal murine CMs varies with substrate stiffness (18, 29).

We used multiple approaches to test the idea that tension varies with shape and substrate stiffness and regulates changes in the contractile output of our engineered hPSC-CMs. To test the effect of substrate stiffness, we made different hydrogels with the stiffness of embryonic myocardium (6 kPa), healthy myocardium (10 kPa), and ischemic or fibrotic myocardium (35 kPa) (13). When cultured on 35-kPa hydrogels, engineered hPSC-CMs generated 90% less $\Sigma|F_c|$ than on 6- and 10-kPa hydrogels (Fig. 3*A*). On 35-kPa hydrogels, 7:1 hPSC-CMs generated higher $\Sigma|F_c|$ than 5:1 hPSC-CMs; however, on 6-kPa hydrogels, $\Sigma|F_c|$ did not differ between 7:1 and 5:1 hPSC-CMs (Fig. 3*A*). Mechanical output was highest on hydrogels with the stiffness of healthy myocardium (6 and 10 kPa). However, intracellular tension also decreases with decreasing substrate stiffness (27), and fewer engineered hPSC-CMs on 6-kPa hydrogels retained their myofibril organization over the contractile cycle but instead exhibited myofibril buckling during relaxation (*SI Appendix*, Fig. S9 and Movies S5–S8). Cells with laterally registered sarcomeres had less myofibril buckling (Movie S9). We next tested whether decreased $\Sigma|F_c|$ on 35-kPa hydrogels also correlated with myofibril disorganization. Myofibrils exhibited discontinuities and were disrupted in ∼25% of cells on 35-kPa hydrogels (Fig. 3*B* and *SI Appendix*, Fig. S10) but not on 6- or 10-kPa substrates.

To test the hypothesis that tension increased above a threshold by stiffer substrates leads to myofibril rupture and decreased mechanical output, we stretched engineered hPSC-CMs with a glass rod to shear the hydrogel proximal to a cell and measured the contractile power output vs. stretch (*SI Appendix*, Fig. S11). Cell power increased for stretches of 5–10% cellular strain but myofibrils ruptured at 14% strain (Fig. 3*C*). Above 14% strain, cells stopped beating or power output decreased. In healthy myocardium, physiological strains up to 10% increase mechanical output (17); primary CMs also only increase output over a limited range of tension (30), above which sarcomere activity also decreases (31). Thus, we asked whether contractility is necessary to drive myofibril rupture in our overloaded cells. Consistent with prior reports (11), myofibrils did not rupture when engineered hPSC-CMs were cultured on glass, where sarcomeres twitched but cells did not shorten with beating (*SI Appendix*, Fig. S12 and Movie S10). To further test the idea that mechanical output decreases on 35 kPa because higher intracellular tension decreases sarcomere

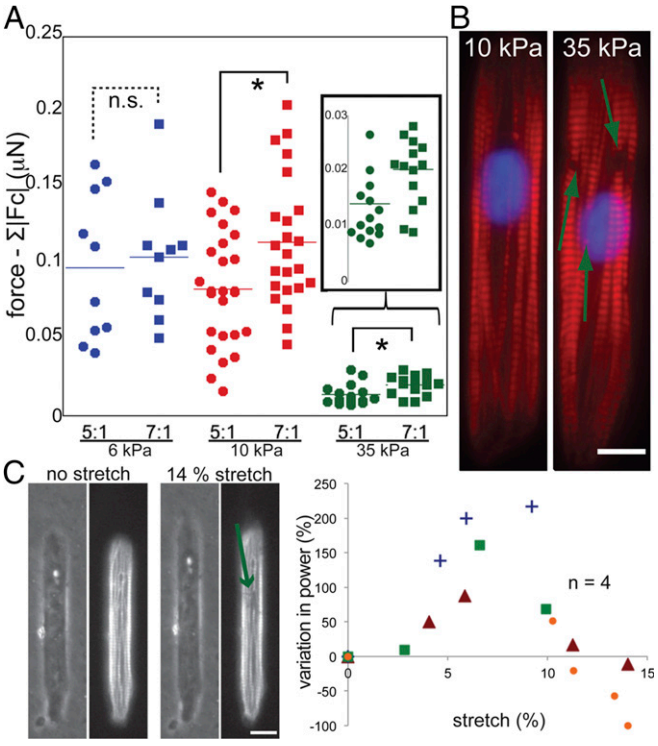

Fig. 3. Substrate stiffness and substrate stretching affect the myofibril integrity and mechanical output of engineered hPSC-CMs. (*A*) hPSC-CMs (7:1) produced higher $\Sigma|F_c|$ than 5:1 cells on 10- and 35-kPa substrates. *$P < 0.01$ by unpaired Wilcoxon–Mann–Whitney rank-sum test; $n > 9$. Each dot indicates one cell. Lines indicate the mean. (*B*) Myofibrils (green arrows) were disrupted in Lifeact-labeled (red) hPSC-CMs cultured on 35-kPa substrates. Blue = nucleus. (Scale bar, 10 μm.) (*C*) (*Left*) Single Lifeact-labeled 7:1 cell under stretch. Myofibrils were disrupted (green arrow), and mechanical force was reduced, at a stretch of 14% of the cell's unstretched length. (Scale bar, 20 μm.) (*Right*) Power generated by single cells increased and then decreased over this range of stretch. *n*, number of stretched cells analyzed. Each symbol is a single cell.

and myofibril activity, we increased contractile activity by increasing the extracellular calcium concentration (*SI Appendix*, Fig. S13*A*) (32). The fraction of hPSC-CMs with disrupted myofibrils (*SI Appendix*, Fig. S13*B* and Movies S11 and S12) increased to 50% (*SI Appendix*, Fig. S13*D*).

To determine whether intracellular tension is needed to maintain myofibril alignment, we incubated patterned hPSC-CMs in EDTA to chelate calcium and reduce integrin-mediated cell-substrate adhesion (33, 34) and disrupt myofibril tension (35) and the intracellular balance of forces. Beating stopped upon EDTA addition, whereas buckling, disruption, and loosening of myofibrils and loss of sarcomere periodic organization increased with incubation (*SI Appendix*, Fig. S14). hPSC-CMs with high myofibril density and sarcomere registration (*SI Appendix*, Fig. S15) resisted myofibril damage and detachment from the substrate for >1 h.

To determine whether myofibrils realign as adhesion and intracellular tension recover, we induced myofibril defects with short-term EDTA incubation and added fresh medium. Myofibril alignment recovered in just 4 h (*SI Appendix*, Fig. S16). We repeated this experiment but added small molecules to the new medium to abrogate intracellular tension. We inhibited cytoskeleton polymerization (nocodazole for microtubules and cytochalasin D for F-actin) or intracellular tension (blebbistatin to block nonmuscle myosin II binding to actin, ML-7 to inhibit nonmuscle myosin light-chain kinase, or BDM to inhibit ATPase of nonmuscle myosin). In the presence of nocodazole, myofibrils realigned after

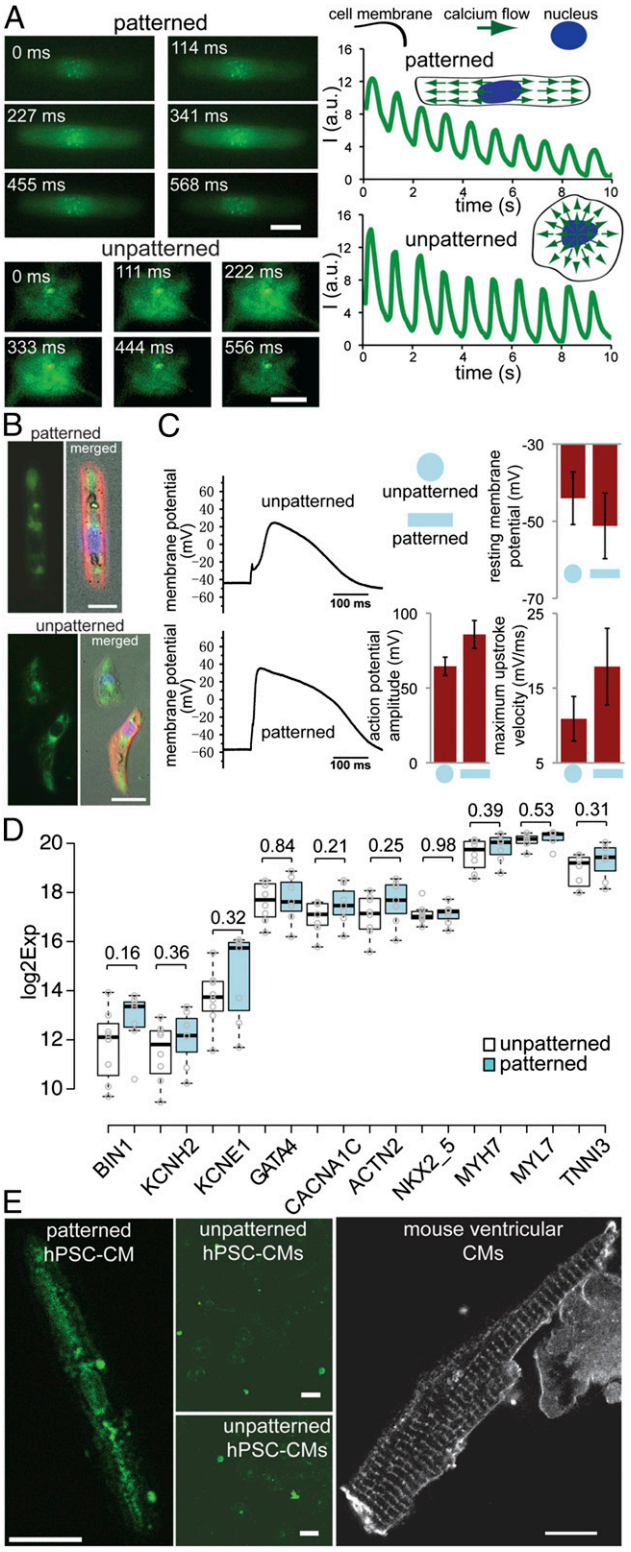

Fig. 4. hPSC-CMs on 7:1 patterns have phenotypes similar to those of mature CMs. (*A*) Labeled calcium (green) flowed along the major axis of 7:1 cells but flowed isotropically in unpatterned cells. Intensity (I) plotted with arbitrary units (a.u.). (Scale bars, 20 μm.) (*B*) Mitochondria were labeled (green) in cells expressing Lifeact (red). The distribution of mitochondria in 7:1 hPSC-CMs differed from that in unpatterned cells. [Scale bars, 20 μm (*Top*) and 50 μm (*Bottom*).] Blue, nuclei. (*C*) (*Left*) Patch-clamp recordings of variations in membrane action potential over time during single-cell contractions. (*Right*) Action potential amplitude, resting membrane potential, and maximum upstroke velocity of seven unpatterned cells and seven 7:1 cells. Means and SDs are shown. (*D*) Single-cell gene expression assayed by qRT-PCR. Centerlines indicate medians; box limits indicate 25th and 75th percentiles; whiskers encompass 1.5 times the interquartile range. (*E*) Cells labeled with di-8-ANEPPS (see *SI Appendix, SI Materials and Methods*). (*Left*) hPSC-CM (7:1). (Scale bar, 25 μm.) (*Center*) Unpatterned hPSC-CM on a 10-kPa hydrogel shown in both *Top* and *Bottom*. (Scale bars, 50 μm.) (*Right*) Isolated adult mouse ventricular CM. (Scale bar, 25 μm.)

EDTA treatment (*SI Appendix*, Fig. S17*A*). Cytochalasin D increased myofibril defects (*SI Appendix*, Fig. S17*B*), as did blebbistatin, ML-7, and BDM (*SI Appendix*, Fig. S18). Cells without EDTA-induced myofibril defects shortened when incubated with ML-7 or BDM for 4 h but their myofibril organization changed little (*SI Appendix*, Fig. S19). Thus, tuned intracellular tension mediated by actomyosin activity is necessary for myofibril alignment. A 7:1 aspect ratio and substrate stiffness of 10 kPa develop the required tension for hPSC-CMs to establish mature myofibrils and contractile function.

We next examined expression of *titin*, which regulates tension along myofibrils (36, 37), and troponin I (TnI) and troponin T (TnT), which regulate sarcomere contraction (38, 39). We compared expression of TnI, TnT, and titin isoforms (N2A and N2B) in unpatterned hPSC-CMs on 10-kPa hydrogels vs. patterned on glass and 10- and 35-kPa hydrogels (*SI Appendix*, Fig. S20). Titin expression did not change in cells patterned on 10 and 35 kPa but differed significantly on patterned and unpatterned hydrogels and patterned hydrogels and glass. N2A expression was highest on unpatterned hydrogels and patterned glass; N2B expression was higher on glass than on unpatterned hydrogels. TnT expression was highest on glass but similar in patterned and unpatterned hydrogels, whereas TnI expression was significantly higher on patterned hydrogels than on glass or unpatterned hydrogels. These results support the notion that substrate stiffness and cell shape act cooperatively to regulate the function of hPSC-CMs via mechanisms known to tune sarcomere tension and contractility.

Improved Mechanical Activity of Sarcomeres Enhances Other Maturity Metrics. Engineered hPSC-CMs have more physiological myofibril alignment, sarcomere lateral registry, cell shape, and direction of contractile movement than unpatterned hPSC-CMs (Figs. 1–3). However, calcium signaling, mitochondrial organization, electrophysiology, gene expression, and t-tubule formation also define the maturity of primary CMs (6, 10). Intracellular calcium regulates cardiac contractility and flows along the major axis of beating primary adult CMs to trigger contractility (40). We saw that calcium flow propagates anisotropically along the major axis in engineered hPSC-CMs but isotropically in unpatterned cells (Fig. 4*A*). Mitochondria were systematically distributed in engineered hPSC-CMs, with higher concentrations around the perinuclear space and cell extremities, but were sparse and randomly distributed in unpatterned hPSC-CMs (Fig. 4*B* and *SI Appendix*, Fig. S21) (6). In primary CMs, mitochondria are homogeneously distributed and occupy up to 60% of the cell volume (41).

To analyze electrophysiology, we made patch-clamp recordings from single cells (Fig. 4*C*). The maturity and type (ventricular, atrial, or nodal) of primary CMs are reflected in the temporal profile of action potentials during contractions. We evaluated hPSC-CMs with a ventricular profile, a cell fate of interest for modeling cardiac activity (42). The engineered cells had lower resting membrane potential, higher action potential amplitude, and higher maximum upstroke velocity than unpatterned cells (Fig. 4*C*) and were thus more similar to ventricular CMs.

Next, we used single-cell quantitative (q)RT-PCR to quantify the relative expression of cardiac maturation genes encoding ion channels, transcription factors, and sarcomere proteins. These genes were expressed at similar levels in engineered and unpatterned single hPSC-CMs (Fig. 4*D*). Thus, the greater maturity of engineered hPSC-CMs was not associated with changes in the expression of

these genes. Primary adult CMs have t-tubules—deep invaginations of the sarcolemma (43) that organize periodically like Z lines and have only been seen in hPSC-CMs in engineered microtissues (32). Engineered single hPSC-CMs had t-tubule–like structures distributed along the cell membrane (Fig. 4*E*), suggesting that improved sarcomere and myofibril maturity are coupled to other maturity markers.

Discussion

This study shows that physiological shape and substrate stiffness increase the translation of sarcomere shortening to mechanical output in hPSC-CMs by setting the necessary intracellular tension that regulates contractility and establishes and maintains myofibril alignment. Sarcomere activity and myofibril alignment were highest in engineered 7:1 hPSC-CMs, which resembled mature CMs in their electrophysiology, direction of calcium flow, organization of mitochondria, and presence of t-tubules. Greater cell maturity seemed to correlate with improved mechanical activity of sarcomeres. Our findings suggest that engineered hPSC-CMs are a biologically suitable model for studying the contractility of human CMs.

Our engineered hPSC-CMs had $\Sigma|F_c|$ similar to that of primary adult CMs (micronewton range) (44) when the extracellular concentration of calcium was increased (*SI Appendix*, Fig. S13*A*). Otherwise, $\Sigma|F_c|$ of 7:1 hPSC-CMs was similar to maximal values reported in other studies of single hPSC-CMs (0.1–500 nN) (45, 46), possibly reflecting the use of different force-measuring techniques and improved myofibril alignment. Sarcomere length varies with cell aspect ratio in murine neonatal CMs micropatterned on glass (16, 20). However, we observed physiological sarcomere lengths around 2 μm and detected no difference in sarcomere length for aspect ratios from 3:1 to 7:1. This may be due to sarcomeric differences of human and murine CMs (8, 9).

Overall, cell function improved with physiological shape on substrates with physiological stiffness (10 kPa). The stiffness of primary adult murine CMs is 10–40 kPa (47), which matches the stiffness of our hydrogels. In contrast, engineered cells on 6- and 35-kPa substrates had defects in myofibril organization through overtension and myofibril rupture (35 kPa) or undertension and myofibril buckling (6 kPa) (48). Previous studies found that 10-kPa substrates yield useful cultures of immature primary neonatal murine CMs with physiological shape (21, 23). Increasing substrate stiffness without controlling cell shape increases the force output of neonatal murine CMs (25) and unpatterned hPSC-CMs (24). We found that variations in stiffness affect the mechanical output of engineered hPSC-CMs by changing myofibril function. Thus, hPSC-CMs grown without shape constraints may adapt to increased substrate stiffness and the resultant increase in intracellular tension by varying their shape and myofibril organization to balance intracellular forces (35).

Our observations support the idea that physiological substrate stiffness and cell shape tune the distribution of intracellular tension necessary for physiological sarcomere activity and mechanical output of hPSC-CMs. Tension is tuned by myofibril alignment and distribution and strength of cell adhesion, which are set by cell shape and substrate stiffness. Tension is also tuned by modified expression and activity of contractile and structural genes downstream of myofibril organization and cell adhesion.

The assembly of actin filaments into contractile stress fibers follows a mechanism common among adherent cell types (49), and actin stress fiber alignment is also seen in other cell types patterned into rectangular shapes (26, 50, 51). Nonmuscle actin stress fibers have several homologies with their myofibril isoforms in contractility, organization, and composition (49, 52, 53). Nonmuscle actin fibers also develop as bipolar linear structures with periodically distributed clusters of α-actinin and myosin (54–56). In developing myocytes, premyofibrils, a muscle-specific type of actin stress fiber, interact with the cell membrane (57–59) and evolve into myofibrils. A rectangular shape prealigns the cell membrane along what will be the major contractile axis. In our engineered hPSC-CMs, mature myofibrils were highly concentrated near the cell membrane and tension was required to establish and maintain myofibril alignment and organization. Intracellular tension was downstream of myofibril distribution and density, actomyosin activity, and cell-adhesion strength (*SI Appendix*, Figs. S14–S19).

Cell adhesions in the extremities of engineered hPSC-CMs anchor myofibrils to the substrate and regulate the tension necessary for contractile function. For adherent cells in general, a rectangular cell shape strengthens substrate adhesions at the extremities (60, 61). Intracellular tension increases with the aspect ratio of cells and is necessary for strong adhesions in cell extremities (26). Substrate stiffness regulates the strength, activity, and stability of cell adhesions to the substrate, and their strength is reflected in the development of intracellular tension to maintain equilibrium of forces (62–64). Our findings are consistent with these observations and with evidence that sarcomere activity in cardiac muscle is regulated by intracellular tension of CMs (30, 31, 65).

The recovery of myofibril alignment after loss of intracellular tension and contractility upon calcium chelation shows a role for shape- and substrate-induced tension in driving myofibrillogenesis and enhanced maturity. The inhibition of tension with small-molecule inhibitors of the actin cytoskeleton and contractility further support the idea that these mechanisms of tension generation are essential for myofibril maturation (*SI Appendix*, Figs. S17–S19). The intracellular tension and contractility of primary CMs also depend on these intra- and extrasarcomeric cytoskeletal structures (1, 31, 36, 39). The expression levels of titin isoforms (N2A and N2B) and TnI and TnT differed in cultures of 7:1 hPSC-CMs on polyacrylamide vs. glass (*SI Appendix*, Fig. S20) and in patterned vs. unpatterned cells. Thus, cells may actively regulate sarcomere proteins to tune tension on these different substrates. Interestingly, the up-regulation of troponins is a marker of heart failure (66). The differential expression of TnT relative to TnI in heart disease (67) supports the idea that differences in their expression are related to CM function. Further study is needed to understand how stiffness and shape regulate the expression of sarcomere proteins.

We expected force to scale with cellular cross-sectional area, and the number of sarcomeres in parallel and velocity to scale with the number of sarcomeres in series. However, we found that contraction velocities are similar across the different cellular aspect ratio. Thus, power scales only with force, which may be due to the constant cell spread area (2,000 μm^2) and imaging at one focal plane. In addition, the alignment and organization of myofibrils are different between hPSC-CMs with different aspect ratios, which affects the translation of sarcomere shortening to force between these cells. Future work should explore variations in cell volume with aspect ratio and spread area, as well as quantification of sarcomeres in patterned hPSC-CMs. Studies of varied volumes and edge shapes will also enable us to test whether increased membrane tension provides the structural cues (68) needed for t-tubule formation (69).

Our findings, along with the developed methods and platforms, will facilitate studies to understand the biomechanics of engineered hPSC-CMs and their use as models of human heart physiology to elucidate CM function and test hypotheses about the causes of heart diseases.

Materials and Methods

We engineered hPSC-CMs on 2,000-μm^2 rectangular Matrigel patterns with aspect ratios (length:width) of 3:1, 5:1, and 7:1 on 10-kPa polyacrylamide substrates (unless noted otherwise). For myofibril imaging and simultaneous quantification of mechanical output, sarcomere activity, and myofibril alignment, cells were transfected with a virus that harbors an RFP-Lifeact expression system. Phenotypes were analyzed with ImageJ (NIH) and MATLAB (MathWorks)-based algorithms from videos of hPSC-CMs contracting under electrical field stimulation at 1 Hz. Full materials and methods are available in *SI Appendix, SI Materials and Methods*.

ACKNOWLEDGMENTS. We thank C. Liu, A. Heidersbach, and E. Booth for discussions. This study was supported by American Heart Association Fellowships 14POST18360018 (to A.J.S.R.) and 13POST17390040 (to Y.-S.A.) and Award 13SDG14580035 (to J.-D.F.), the National Science Foundation under MIKS-1136790 (to B.L.P.), the National Institutes of Health under R01-EB006745 (to B.L.P.), and seed grants from the Stanford Cardiovascular Institute and Bio-X.

1. Dorn GW, II, Molkentin JD (2004) Manipulating cardiac contractility in heart failure: Data from mice and men. *Circulation* 109(2):150–158.
2. Louch WE, Sheehan KA, Wolska BM (2011) Methods in cardiomyocyte isolation, culture, and gene transfer. *J Mol Cell Cardiol* 51(3):288–298.
3. de Tombe PP, ter Keurs HE (2012) The velocity of cardiac sarcomere shortening: Mechanisms and implications. *J Muscle Res Cell Motil* 33(6):431–437.
4. Lodish HF, et al. (2012) Myosin-powered movements. Molecular Cell Biology (W. H. Freeman, New York), 7th Ed, pp 801–805.
5. Knöll R, Buyandelger B, Lab M (2011) The sarcomeric Z-disc and Z-discopathies. *J Biomed Biotechnol* 2011:569628.
6. Yang X, Pabon L, Murry CE (2014) Engineering adolescence: Maturation of human pluripotent stem cell-derived cardiomyocytes. *Circ Res* 114(3):511–523.
7. Parameswaran S, Kumar S, Verma RS, Sharma RK (2013) Cardiomyocyte culture—An update on the in vitro cardiovascular model and future challenges. *Can J Physiol Pharmacol* 91(12):985–998.
8. Reiser PJ, Portman MA, Ning XH, Schomisch Moravec C (2001) Human cardiac myosin heavy chain isoforms in fetal and failing adult atria and ventricles. *Am J Physiol Heart Circ Physiol* 280(4):H1814–H1820.
9. Milani-Nejad N, Janssen PM (2014) Small and large animal models in cardiac contraction research: Advantages and disadvantages. *Pharmacol Ther* 141(3):235–249.
10. Sheehy SP, et al. (2014) Quality metrics for stem cell-derived cardiac myocytes. *Stem Cell Rep* 2(3):282–294.
11. Wang G, et al. (2014) Modeling the mitochondrial cardiomyopathy of Barth syndrome with induced pluripotent stem cell and heart-on-chip technologies. *Nat Med* 20(6): 616–623.
12. French A, et al. (2015) Enabling consistency in pluripotent stem cell-derived products for research and development and clinical applications through material standards. *Stem Cells Transl Med* 4(3):217–223.
13. Engler AJ, et al. (2008) Embryonic cardiomyocytes beat best on a matrix with heart-like elasticity: Scar-like rigidity inhibits beating. *J Cell Sci* 121(Pt 22):3794–3802.
14. Hughes CS, Postovit LM, Lajoie GA (2010) Matrigel: A complex protein mixture required for optimal growth of cell culture. *Proteomics* 10(9):1886–1890.
15. Boudou T, et al. (2012) A microfabricated platform to measure and manipulate the mechanics of engineered cardiac microtissues. *Tissue Eng Part A* 18(9-10):910–919.
16. Bray MA, Sheehy SP, Parker KK (2008) Sarcomere alignment is regulated by myocyte shape. *Cell Motil Cytoskeleton* 65(8):641–651.
17. Trayanova NA, Rice JJ (2011) Cardiac electromechanical models: From cell to organ. *Front Physiol* 2:43.
18. Chopra A, Tabdanov E, Patel H, Janmey PA, Kresh JY (2011) Cardiac myocyte remodeling mediated by N-cadherin-dependent mechanosensing. *Am J Physiol Heart Circ Physiol* 300(4):H1252–H1266.
19. Riedl J, et al. (2008) Lifeact: A versatile marker to visualize F-actin. *Nat Methods* 5(7): 605–607.
20. Kuo PL, et al. (2012) Myocyte shape regulates lateral registry of sarcomeres and contractility. *Am J Pathol* 181(6):2030–2037.
21. McCain ML, Yuan H, Pasqualini FS, Campbell PH, Parker KK (2014) Matrix elasticity regulates the optimal cardiac myocyte shape for contractility. *Am J Physiol Heart Circ Physiol* 306(11):H1525–H1539.
22. Friedrich BM, Buxboim A, Discher DE, Safran SA (2011) Striated acto-myosin fibers can reorganize and register in response to elastic interactions with the matrix. *Biophys J* 100(11):2706–2715.
23. Chopra A, et al. (2012) Reprogramming cardiomyocyte mechanosensing by crosstalk between integrins and hyaluronic acid receptors. *J Biomech* 45(5):824–831.
24. Hazeltine LB, et al. (2012) Effects of substrate mechanics on contractility of cardiomyocytes generated from human pluripotent stem cells. *Int J Cell Biol* 2012: 508294.
25. Hersch N, et al. (2013) The constant beat: Cardiomyocytes adapt their forces by equal contraction upon environmental stiffening. *Biol Open* 2(3):351–361.
26. Oakes PW, Banerjee S, Marchetti MC, Gardel ML (2014) Geometry regulates traction stresses in adherent cells. *Biophys J* 107(4):825–833.
27. Mih JD, Marinkovic A, Liu F, Sharif AS, Tschumperlin DJ (2012) Matrix stiffness reverses the effect of actomyosin tension on cell proliferation. *J Cell Sci* 125(Pt 24): 5974–5983.
28. Banerjee S, Sknepnek R, Marchetti MC (2014) Optimal shapes and stresses of adherent cells on patterned substrates. *Soft Matter* 10(14):2424–2430.
29. Young JL, Kretchmer K, Ondeck MG, Zambon AC, Engler AJ (2014) Mechanosensitive kinases regulate stiffness-induced cardiomyocyte maturation. *Sci Rep* 4:6425.
30. ter Keurs HE, Rijnsburger WH, van Heuningen R, Nagelsmit MJ (1980) Tension development and sarcomere length in rat cardiac trabeculae. Evidence of length-dependent activation. *Circ Res* 46(5):703–714.
31. Granzier HL, Irving TC (1995) Passive tension in cardiac muscle: Contribution of collagen, titin, microtubules, and intermediate filaments. *Biophys J* 68(3):1027–1044.
32. Godier-Furnémont AF, et al. (2015) Physiologic force-frequency response in engineered heart muscle by electromechanical stimulation. *Biomaterials* 60:82–91.
33. Sjaastad MD, Nelson WJ (1997) Integrin-mediated calcium signaling and regulation of cell adhesion by intracellular calcium. *BioEssays* 19(1):47–55.
34. Zhang K, Chen J (2012) The regulation of integrin function by divalent cations. *Cell Adhes Migr* 6(1):20–29.
35. Mullen CA, et al. (2014) Cell morphology and focal adhesion location alters internal cell stress. *J R Soc Interface* 11(101):20140885.
36. Cazorla O, et al. (2000) Differential expression of cardiac titin isoforms and modulation of cellular stiffness. *Circ Res* 86(1):59–67.
37. Kass DA, Bronzwaer JG, Paulus WJ (2004) What mechanisms underlie diastolic dysfunction in heart failure? *Circ Res* 94(12):1533–1542.
38. Solaro RJ (2003) The special structure and function of troponin I in regulation of cardiac contraction and relaxation. *Adv Exp Med Biol* 538:389–401, discussion 401–402.
39. McCall SJ, et al. (2006) Development and cardiac contractility: Cardiac troponin T isoforms and cytosolic calcium in rabbit. *Pediatr Res* 60(3):276–281.
40. Bers DM (2000) Calcium fluxes involved in control of cardiac myocyte contraction. *Circ Res* 87(4):275–281.
41. Piquereau J, et al. (2013) Mitochondrial dynamics in the adult cardiomyocytes: Which roles for a highly specialized cell? *Front Physiol* 4:102.
42. Winslow RL, et al. (2011) Integrative modeling of the cardiac ventricular myocyte. *Wiley Interdiscip Rev Syst Biol Med* 3(4):392–413.
43. Ibrahim M, Gorelik J, Yacoub MH, Terracciano CM (2011) The structure and function of cardiac t-tubules in health and disease. *Proc Biol Sci* 278(1719):2714–2723.
44. Korte FS, Herron TJ, Rovetto MJ, McDonald KS (2005) Power output is linearly related to MyHC content in rat skinned myocytes and isolated working hearts. *Am J Physiol Heart Circ Physiol* 289(2):H801–H812.
45. Taylor RE, et al. (2013) Sacrificial layer technique for axial force post assay of immature cardiomyocytes. *Biomed Microdevices* 15(1):171–181.
46. Rodriguez ML, et al. (2014) Measuring the contractile forces of human induced pluripotent stem cell-derived cardiomyocytes with arrays of microposts. *J Biomech Eng* 136(5):051005.
47. Chang WT, Yu D, Lai YC, Lin KY, Liau I (2013) Characterization of the mechanodynamic response of cardiomyocytes with atomic force microscopy. *Anal Chem* 85(3): 1395–1400.
48. Bathe M, Heussinger C, Claessens MM, Bausch AR, Frey E (2008) Cytoskeletal bundle mechanics. *Biophys J* 94(8):2955–2964.
49. Tojkander S, Gateva G, Lappalainen P (2012) Actin stress fibers—Assembly, dynamics and biological roles. *J Cell Sci* 125(Pt 8):1855–1864.
50. Roca-Cusachs P, et al. (2008) Micropatterning of single endothelial cell shape reveals a tight coupling between nuclear volume in G1 and proliferation. *Biophys J* 94(12): 4984–4995.
51. Wang D, et al. (2014) Tissue-specific mechanical and geometrical control of cell viability and actin cytoskeleton alignment. *Sci Rep* 4:6160.
52. Peterson LJ, et al. (2004) Simultaneous stretching and contraction of stress fibers in vivo. *Mol Biol Cell* 15(7):3497–3508.
53. Ono S (2010) Dynamic regulation of sarcomeric actin filaments in striated muscle. *Cytoskeleton (Hoboken)* 67(11):677–692.
54. Langanger G, et al. (1986) The molecular organization of myosin in stress fibers of cultured cells. *J Cell Biol* 102(1):200–209.
55. Cramer LP, Siebert M, Mitchison TJ (1997) Identification of novel graded polarity actin filament bundles in locomoting heart fibroblasts: Implications for the generation of motile force. *J Cell Biol* 136(6):1287–1305.
56. Butt T, et al. (2010) Myosin motors drive long range alignment of actin filaments. *J Biol Chem* 285(7):4964–4974.
57. Rhee D, Sanger JM, Sanger JW (1994) The premyofibril: Evidence for its role in myofibrillogenesis. *Cell Motil Cytoskeleton* 28(1):1–24.
58. LoRusso SM, Rhee D, Sanger JM, Sanger JW (1997) Premyofibrils in spreading adult cardiomyocytes in tissue culture: Evidence for reexpression of the embryonic program for myofibrillogenesis in adult cells. *Cell Motil Cytoskeleton* 37(3):183–198.
59. Dabiri GA, Turnacioglu KK, Sanger JM, Sanger JW (1997) Myofibrillogenesis visualized in living embryonic cardiomyocytes. *Proc Natl Acad Sci USA* 94(17):9493–9498.
60. Lemmon CA, Romer LH (2010) A predictive model of cell traction forces based on cell geometry. *Biophys J* 99(9):L78–L80.
61. Banerjee S, Marchetti MC (2013) Controlling cell–matrix traction forces by extracellular geometry. *New J Phys* 15:035015.
62. Pelham RJ, Jr, Wang Yl (1997) Cell locomotion and focal adhesions are regulated by substrate flexibility. *Proc Natl Acad Sci USA* 94(25):13661–13665.
63. Huang J, Peng X, Xiong C, Fang J (2011) Influence of substrate stiffness on cell-substrate interfacial adhesion and spreading: A mechano-chemical coupling model. *J Colloid Interface Sci* 355(2):503–508.
64. Yeung T, et al. (2005) Effects of substrate stiffness on cell morphology, cytoskeletal structure, and adhesion. *Cell Motil Cytoskeleton* 60(1):24–34.
65. Solaro RJ (2011) Left ventricular diastolic and systolic pressure, ejection, and relaxation reflect sarcomeric mechanical properties. *Regulation of Cardiac Contractility,* eds Granger DN, Granger J (Morgan & Claypool Life Sciences, San Rafael, CA), pp 12–14.
66. Maynard SJ, Menown IB, Adgey AA (2000) Troponin T or troponin I as cardiac markers in ischaemic heart disease. *Heart* 83(4):371–373.
67. Rittoo D, Jones A, Lecky B, Neithercut D (2014) Elevation of cardiac troponin T, but not cardiac troponin I, in patients with neuromuscular diseases: Implications for the diagnosis of myocardial infarction. *J Am Coll Cardiol* 63(22):2411–2420.
68. Parton RG, del Pozo MA (2013) Caveolae as plasma membrane sensors, protectors and organizers. *Nat Rev Mol Cell Biol* 14(2):98–112.
69. Sens P, Turner MS (2004) Theoretical model for the formation of caveolae and similar membrane invaginations. *Biophys J* 86(4):2049–2057.